First-principles study of the pressure and crystal-structure dependences of the superconducting transition temperature in compressed sulfur hydrides

Ryosuke Akashi,[1,*] Mitsuaki Kawamura,[1] Shinji Tsuneyuki,[1,2] Yusuke Nomura,[3,4] and Ryotaro Arita[3,5]

[1]*Department of Physics, The University of Tokyo, Hongo, Bunkyo-ku, Tokyo 113-0033, Japan*

[2]*Institute of Solid State Physics, The University of Tokyo, Kashiwa, Chiba 277-8581, Japan*

[3]*RIKEN Center for Emergent Matter Science, Wako, Saitama 351-0198, Japan*

[4]*Department of Applied Physics, The University of Tokyo, Hongo, Bunkyo-ku, Tokyo 113-8656, Japan*

[5]*JST ERATO Isobe Degenerate π-Integration Project, Advanced Institute for Materials Research (AIMR), Tohoku University, Sendai, Miyagi 980-8577, Japan*

(Received 3 February 2015; revised manuscript received 9 June 2015; published 30 June 2015)

We calculate the superconducting transition temperatures (T_c) in sulfur hydrides H_2S and H_3S from first principles using the density functional theory for superconductors. At pressures of $\lesssim$150 GPa, the high values of T_c ($\geqslant$130 K) observed in a recent experiment (A. P. Drozdov, M. I. Eremets, and I. A. Troyan, arXiv:1412.0460) are accurately reproduced by assuming that H_2S decomposes into $R3m$ H_3S and S. For higher pressures, the calculated T_c's for $Im\bar{3}m$ H_3S are systematically higher than those for $R3m$ H_3S and the experimentally observed maximum value (190 K), which suggests the possibility of another higher-T_c phase. We also quantify the isotope effect from first principles and demonstrate that the isotope effect coefficient can be larger than the conventional value (0.5) when multiple structural phases energetically compete.

DOI: 10.1103/PhysRevB.91.224513 PACS number(s): 74.62.Fj, 74.20.−z, 74.25.Kc, 74.70.−b

I. INTRODUCTION

Investigating compounds containing light elements has been a simple and powerful guiding principle for the discovery of high-temperature superconductors. According to the BCS theory [1], the superconducting transition temperature (T_c) is scaled by the phonon frequency and therefore light atoms are advantageous for achieving high T_c. Despite its simplicity, this principle has been surprisingly successful, as represented by the discoveries of superconductivity in doped fullerene solids [2], magnesium diboride [3], lithium under pressure [4,5], and boron-doped diamond [6,7]. Along this principle, possible superconductivity in compressed hydrogen and hydrogen compounds has been explored as an extreme case [8–35].

Recently, it has been discovered that H_2S exhibits superconductivity under high pressures at 190 K [36]. Since it is a new record of the superconducting transition temperature (T_c), this report has immediately aroused intense debate [37–41]. Several facts imply that this superconducting phase is induced by the conventional mechanism due to the vibrations of hydrogen atoms: The observed T_c is subject to the hydrogen isotope effect [36]; prior to the experimental discovery, there was an *ab initio* calculation which predicted a strong electron-phonon coupling [34]; the electronic bandwidth is so large that the Migdal approximation seems valid [42]. However, some puzzling results have also been exposed. First, the crystal structure realized in the experimental situation has not been specified. If we estimate T_c of H_2S using the conventional McMillan formula [34,43] with the empirical Coulomb parameter $\mu^* = 0.13$, the calculated value is too low compared with the experimentally observed value. It has also been proposed that, instead, the H_3S phase emerges under high pressures [39,41], where the electron-phonon coupling is thought to be stronger than in H_2S [35]. Second, an anomalously large hydrogen isotope effect coefficient $\alpha \sim 1.0$ has been observed. Although it has been hypothesized that the anharmonic effect on the lattice dynamics plays some role [41] or that different structures emerge in H_2S and D_2S (sulfur dideuteride) [37], this anomaly remains an open question.

To further investigate the above points, we need to address not only the electron-phonon interaction but also the electron-electron Coulomb interaction in H_xS systems. An accurate evaluation of the impact of the pair-breaking Coulomb repulsion is vital because this governs the absolute value of T_c, as well as α [44–46]. In addition, an experimentally realized pressure range is rather out of the range investigated in previous *ab initio* studies, and therefore more thorough investigations of the pressure dependence of the superconducting properties are desired.

In this paper, we present an *ab initio* study on the superconductivity in solid H_2S and H_3S covering the experimental pressure range. In the standard Migdal-Eliashberg theory [42,47], the effect of the electron-electron Coulomb interaction is treated practically with an empirical parameter μ^*. To incorporate this effect nonempirically, we utilize the density functional theory for superconductors (SCDFT [48,49]). With this theory, we can calculate T_c and α without any empirical parameter, which can be directly compared with the experimental data.

II. METHOD

To calculate T_c from first principles, we employed the SCDFT gap equation given by

$$\Delta_{n\mathbf{k}} = -\mathcal{Z}_{n\mathbf{k}}\Delta_{n\mathbf{k}} - \frac{1}{2}\sum_{n'\mathbf{k}'}\mathcal{K}_{n\mathbf{k}n'\mathbf{k}'}\frac{\tanh[(\beta/2)E_{n'\mathbf{k}'}]}{E_{n'\mathbf{k}'}}\Delta_{n'\mathbf{k}'}. \quad (1)$$

*Author to whom correspondence should be addressed: akashi@cms.phys.s.u-tokyo.ac.jp

Here, n and $\mathbf{k}$ denote the band index and crystal momentum, respectively, $\Delta_{n\mathbf{k}}$ is the gap function, and β is the inverse temperature. The energy $E_{n\mathbf{k}}$ is defined as $E_{n\mathbf{k}} = \sqrt{\xi_{n\mathbf{k}}^2 + \Delta_{n\mathbf{k}}^2}$ and $\xi_{n\mathbf{k}}$ is the one-electron energy with respect to the Fermi level calculated with the normal Kohn-Sham equation. The functions $\mathcal{Z}$ and $\mathcal{K}$ are called exchange-correlation kernels, which describe the effects of the interactions. The nondiagonal kernel $\mathcal{K}$ consists of two parts $\mathcal{K} = \mathcal{K}^{\rm ph} + \mathcal{K}^{\rm el}$ representing the electron-phonon and electron-electron interactions, respectively. The diagonal kernel $\mathcal{Z} = \mathcal{Z}^{\rm ph}$ represents the mass renormalization of the normal-state band structure due to the phonon exchange. Using these kernels [48,49], the conventional strong-coupling superconductivity can be treated with a level of the Migdal-Eliashberg theory [42,47]. In particular, the electronic nondiagonal kernel $\mathcal{K}^{\rm el}$ describes the screened electron-electron Coulomb interaction, where the dynamical screening effects are incorporated within the random-phase approximation [50,51]. We can therefore evaluate the effects of the static Coulomb repulsion suppressing the pairing, as well as the plasmon superconducting mechanism [52].

We calculated the electronic states, phonon frequencies, electron-phonon and electron-electron interactions, and T_c for H_2S and H_3S at various pressures. Our calculations were performed within the generalized-gradient approximation using the exchange-correlation potential with the Perdew-Burke-Ernzerhof parametrization [53]. We used the *ab initio* plane-wave pseudopotential calculation codes QUANTUM ESPRESSO [54] for the electronic structure, dynamical matrix, and electron-phonon coupling. The input crystal structures at respective pressures were the optimum ones predicted in previous *ab initio* calculations, which are summarized in Table I. For all the conditions, we optimized the atomic configurations and cell parameters with respect to enthalpy under fixed pressures. Phonon frequencies and electron-phonon interactions were calculated based on the density functional perturbation theory [55]. The electron dielectric functions were calculated within the random-phase approximation, where the frequency dependence was retained. $\mathcal{K}^{\rm ph}$ and $\mathcal{Z}^{\rm ph}$ were calculated with the $n\mathbf{k}$-averaged approximate formula [Eq. (23) in Ref. [49] and Eq. (40) in Ref. [56], respectively], whereas $\mathcal{K}^{\rm el}$ was calculated including the plasmon-induced dynamical screening effect [50,51]. The SCDFT gap equation was solved with the random sampling scheme given in Ref. [57], with which the sampling error was approximately a few percent. Further details are summarized in Appendix A.

TABLE I. Pressure settings and the corresponding input structures for the calculations. We observed that it is difficult to achieve the numerical convergence in the phonon calculations for the calculations for H_3S at 190 GPa since it is near the second-order structural transition point [35].

P (GPa)	130	150	170	190	210	230	250
H_2S	$P1$ [34]		$Cmca$ [34]				
H_3S	$R3m$ [35]			...	$Im\bar{3}m$ [35]		

We took particular care in calculating the Eliashberg function,

$$\alpha^2 F(\omega) = \frac{1}{N(0)} \sum_{\substack{\nu\mathbf{q} \\ nn'\mathbf{k}}} \left| g_{\nu\mathbf{q}}^{n\mathbf{k}+\mathbf{q},n'\mathbf{k}} \right|^2 \delta(\xi_{n\mathbf{k}+\mathbf{q}}) \delta(\xi_{n'\mathbf{k}}) \delta(\omega - \omega_{\nu\mathbf{q}}), \tag{2}$$

employed for $\mathcal{K}^{\rm ph}$ and $\mathcal{Z}^{\rm ph}$. $N(0)$, $g_{\nu\mathbf{q}}^{n\mathbf{k}+\mathbf{q},n'\mathbf{k}}$, and $\omega_{\nu\mathbf{q}}$ denote the density of states at the Fermi energy, the electron-phonon matrix element, and the phonon frequency, respectively. Since we have found that $\alpha^2 F(\omega)$ sensitively depends on the smearing scheme and $\mathbf{k}$- and $\mathbf{q}$-point density for the integration, we employed a recently developed tetrahedron method with an optimized linear interpolation [58].

We included the plasmon-induced frequency dependence of the screened Coulomb interaction in $\mathcal{K}^{\rm el}$ with the following formula [Eq. (2) of Ref. [50]],

$$\mathcal{K}_{n\mathbf{k},n'\mathbf{k}}^{\rm el,dyn} = \lim_{\Delta_{n\mathbf{k}} \to 0} \frac{1}{\tanh[(\beta/2)E_{n\mathbf{k}}]} \frac{1}{\tanh[(\beta/2)E_{n'\mathbf{k}'}]} \frac{1}{\beta^2} \times \sum_{\omega_1 \omega_2} F_{n\mathbf{k}}(i\omega_1) F_{n\mathbf{k}}(i\omega_2) W_{n\mathbf{k}n'\mathbf{k}'}[i(\omega_1 - \omega_2)], \tag{3}$$

where $W_{n\mathbf{k}n'\mathbf{k}'}[i(\omega_1 - \omega_2)]$ is the screened Coulomb interaction and $F_{n\mathbf{k}}(i\omega) = \frac{1}{i\omega + E_{n\mathbf{k}}} - \frac{1}{i\omega - E_{n\mathbf{k}}}$ denotes the electronic anomalous Green's function. In the previous calculations [50,51], we carried out the Matsubara summations analytically by approximating $W_{n\mathbf{k}n'\mathbf{k}'}[i(\omega_1 - \omega_2)]$ with model functions. In the present study, the summation for ω_1 was done analytically with a variable transformation $\omega_1 - \omega_2 \equiv \nu$, whereas the summation for ν was evaluated numerically with $\sum_\nu \sim \frac{1}{T} \int d\nu$ without any modeling of $W_{n\mathbf{k}n'\mathbf{k}'}[d(\omega_1 - \omega_2)]$, where T is the temperature [59].

III. RESULTS AND DISCUSSION

Below, we show the calculated values of T_c and key factors for the phonon theory: λ, $\omega_{\ln}$, μ^*, and the isotope effect coefficient α. The specific values are summarized in Appendix B.

In Fig. 1, we show the calculated T_c with the previously published experimental and first-principles numerical data [34–36]. Drozdov and co-workers [36] reported two data groups obtained with different experimental conditions, which are indicated by the open square and circle, respectively; in this work, we refer to these groups as data 1 and data 2, respectively. The calculated T_c's for H_2S (solid square) and H_3S (solid circle) were $\sim$50 and $\geqslant$130 K, respectively. For both H_2S and H_3S, the calculated T_c's show a domelike dependence on the pressure. The maximum T_c's are achieved near the theoretically proposed structural transition points [34,35]. Our calculated values are as a whole in good agreement with previous estimates found with the McMillan-Allen-Dynes formula (Refs. [34,35]). Notably, for H_3S, we obtained 267 K at maximum, which is larger by $\sim$60 K from the previous estimate [35] at 200 GPa. This difference is discussed more specifically later. In the low-pressure regime, the calculated T_c for H_2S (H_3S) agrees well with data 1 (data 2). In the high-pressure regime, on the other hand, the calculated values

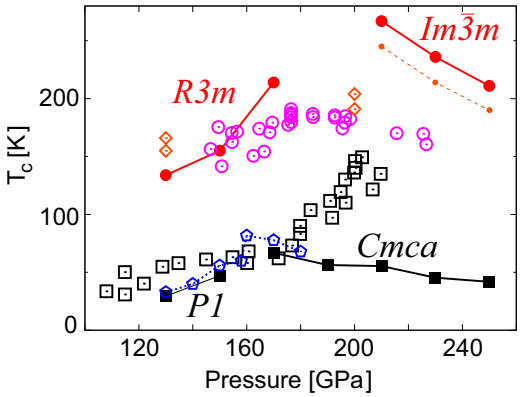

FIG. 1. (Color online) Calculated superconducting transition temperatures for H_2S (solid square) and H_3S (solid circle). Experimentally observed values for H_2S [Fig. 2(a) (open square) and Fig. 2(b) (open circle) of Ref. [36]] are also plotted together, where different runs are represented by the same symbols. The open pentagon and diamond denote the *ab initio* predictions for H_2S [34] and H_3S [35], respectively. The small solid circle for the $Im\bar{3}m$ H_3S phase indicates the calculated result without a contribution from the plasmon mechanism.

are too high or too low compared with the experimental ones. Furthermore, the rapidly increasing feature of data 1 ($\gtrsim$170 GPa) was not reproduced. We also revisit this point later. Regarding the plasmon effect [50,51], the enhancement of T_c was estimated to be 15%–20% ($\sim$10%) for H_2S (H_3S) (e.g., see the small solid circle).

To understand the pressure dependence of the calculated T_c in terms of the McMillan-Allen-Dynes formula [43], we show the calculated values of $\lambda = 2\int d\omega \frac{\alpha^2F(\omega)}{\omega}$ and $\omega_{\ln} = \exp\left[\frac{2}{\lambda}\int d\omega \frac{\alpha^2F(\omega)\ln\omega}{\omega}\right]$ in Figs. 2(a) and 2(b), respectively. We see that the pressure dependences of the present *ab initio* T_c's for H_2S and H_3S are similar to those of λ, which indicates that the T_c's of the present systems are governed by λ. With this plot for λ, we see that our tetrahedron method [58] and the previously employed Gaussian smearing scheme [35,60] give different values for λ, which results in a large difference in T_c. In fact, by calculating λ with the first-order Hermite-Gaussian approximate function $[\delta(\xi) \simeq \frac{1}{\sqrt{\pi}W}[3/2 - (\xi/W)^2]\exp[-(\xi/W)^2]$ with $W = 0.030$ Ry [60], we obtained $\lambda = 2.23$ and 1.99 for $P = 200$ and 210 GPa, respectively, which is consistent with the previous value ($\lambda = 2.19$ for $P = 200$ GPa [35]). Since the bandwidth of the electronic states is extremely large and complex-shaped electron/hole pockets emerge in this system [35], the present tetrahedron-interpolation-based method is expected to be more numerically accurate. We have confirmed the numerical convergence of λ as depicted in Fig. 3. $\omega_{\ln}$ monotonically increases as the pressure is increased, which represents the hardening of phonons by compression. This hardening is responsible for the marked difference in T_c's for $R3m$ H_3S and $Im\bar{3}m$ H_3S. For the higher-pressure regime, however, the hardening is dominated by the decrease of λ and therefore T_c decreases [41].

We determined the optimum values for μ^* so that the T_c's calculated with the SCDFT gap equation can be reproduced

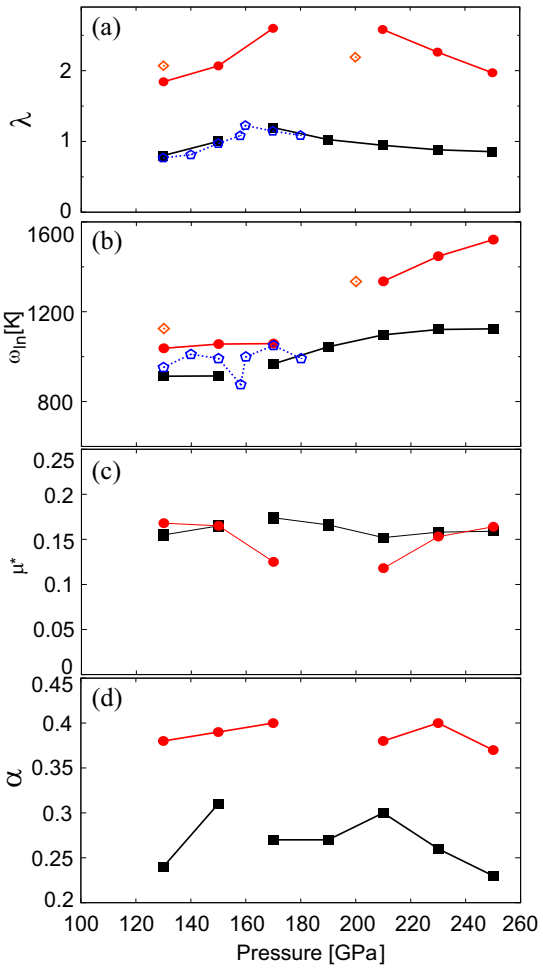

FIG. 2. (Color online) Key factors in the conventional theory for the phonon mechanism calculated from first principles: (a) λ, (b) $\omega_{\ln}$, (c) μ^*, and (d) α. The solid square (circle) denotes the values for H_2S (H_3S). The open pentagon and diamond represent the preceding *ab initio* calculations for H_2S [34] and H_3S [35], respectively.

with the extended McMillan formula [43]. For H_2S, the optimum values were 0.15–0.17 for all the pressures. For the pressure range 170–210 GPa, we observed a decrease of the

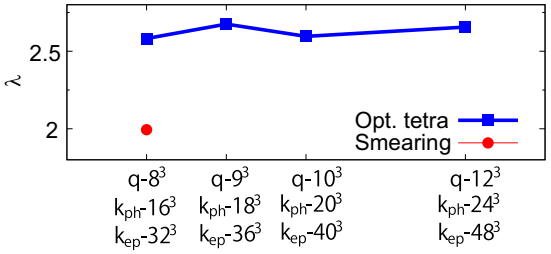

FIG. 3. (Color online) Numerical convergence of λ with different schemes for the phonon and $\alpha^2F(\omega)$ calculations: Optimized tetrahedron and the first-order Hermite-Gaussian smearing with a width of 0.030 Ry. $\mathbf{k}_{\rm ph}$ and $\mathbf{k}_{\rm ep}$ represent the k-point grids employed for the phonon dynamical matrix and Eliashberg function, respectively. The $\mathbf{q}$-point summation for "smearing" was done with a $\mathbf{q}$-point grid without offset.

optimum values for H_3S. Probably this originates from the fact that T_c calculated by the present SCDFT sometimes deviates slightly from that calculated by the Eliashberg equation [48]. Detailed investigations on this point are left for future studies.

Using the calculated T_c's for H_xS and D_xS, we also calculated the isotope effect coefficient $\alpha = -[\ln T_c^{D_xS} - \ln T_c^{H_xS}]/[\ln M_D - \ln M_H]$, where $T_c^{H_xS}$ ($T_c^{D_xS}$) is the transition temperature of the hydride (deuteride) compound and M_H (M_D) is the atomic mass of hydrogen (deuterium), respectively. The values ranges between 0.23 and 0.31 (0.38 and 0.42) for H_2S (H_3S). These values are smaller than the BCS value ($\alpha \sim 0.5$), which indicate the correction due to the retardation effect.

Here we compare our calculated and experimentally observed values of T_c. First, the experimentally observed T_c's in the low-pressure regime were quantitatively reproduced by assuming the emergence of single structural phases of $P1$ H_2S and $R3m$ H_3S for data 1 and 2, respectively. This strongly suggests that these two phases are dominant in the experimental situations for $P \lesssim 150$ GPa. It is even conceivable that the high-pressure values of data 2 correspond to $R3m$ H_3S. The agreement of the calculated and experimentally observed T_c's for higher pressures were, on the other hand, not as perfect as those for the previously studied conventional superconductors [49,50,61–64]. Note that we assumed that the sample is homogeneous and does not decompose into H_xS and S for the entire pressure range, though it has not been confirmed experimentally. Our calculated T_c for $Im\bar{3}m$ H_3S suggests that maximum T_c can be increased to, possibly, a higher value in the pure $Im\bar{3}m$ H_3S phase.

Very recently, there has been an independent report on an *ab initio* T_c calculation for $Im\bar{3}m$ H_3S using the SCDFT [65] with a condition different from ours [66]. They concluded that the experimentally observed high T_c can be explained with $Im\bar{3}m$ H_3S, whereas we propose a relevance of $R3m$ H_3S in the experimental situation.

Finally, we move on to α. The calculated values were far smaller than the experimentally observed $\alpha \sim 1.0$. Based on a hypothesis of inhomogeneity, let us give a possible explanation for the experimentally large α within the present framework. As suggested by Hirsch and Marsiglio [37], when the inhomogeneity of the system is substantial, the experimentally observed T_c should somehow deviate. For example, suppose we estimate α with $\alpha = -[\ln T_c^{D_2S} - \ln T_c^{H_3S}]/[\ln M_D - \ln M_H]$; we then get $\alpha \gtrsim 2.0$ for the whole pressure range. Such a situation is possible because the enthalpy difference between H_2S and $\frac{2}{3}H_3S + \frac{1}{3}S$ is of order of the phonon frequency [39]: A substitution of D for H substantially modulates the contribution of the zero-point oscillation to the total enthalpy, and it should change the relative stability of the competing phases.

We thus suggest that the H_3S phases play a key role in understanding the reported experimental results [36] and realizing higher T_c. To validate or invalidate this, measurements with different chemical compositions (e.g., H : S = 3 : 1) and compression at higher temperatures might be helpful. When measuring the isotope effect, the difference in the structural relaxation speed of hydrides and deuterides should also be taken into account.

IV. SUMMARY

In this study, we have performed a present state-of-the-art *ab initio* calculation for the superconductivity in H_2S and H_3S assuming a conventional phonon mechanism, where the effect of the electron-electron Coulomb repulsion was nonempirically treated. For pressures $\lesssim$150 GPa, the calculated T_c's for $P1$ H_2S and $R3m$ H_3S agree well with the experimental T_c's observed with different compressing and cooling conditions, respectively. This strengthens the scenario that H_3S is superconducting when high T_c is observed [39,40]. For the high-pressure phase of $Im\bar{3}m$ H_3S, we have predicted T_c to be higher than the experimentally observed maximum of 190 K and the values calculated for $R3m$ H_3S, which amounts to 267 K. This suggests that higher T_c can be achieved by isolating the single $Im\bar{3}m$ H_3S phase. Although we have ignored several possible effects in the present systems (e.g., zero-point oscillation of hydrogen atoms, anharmonic phonons, etc.), the present result can be a key step for further theoretical and experimental investigations on superconducting sulfur hydrides. Examinations of anharmonic lattice-dynamical effects, which have been neglected with the present methodology, are under way.

Note added. Recently, we became aware of a publication demonstrating that the anharmonic effect reduces T_c by about 20% in $Im\bar{3}m$ H_3S [69]. Nevertheless, the present indications of the relevance of the $R3m$ phase and a possibly higher T_c are still valid since the increase of T_c by the plasmon mechanism will compensate the anharmonic effect.

ACKNOWLEDGMENTS

This work is partially supported by Tokodai Institute for Element Strategy (TIES) funded by MEXT Elements Strategy Initiative to Form Core Research Center. Y.N. is supported by Grant-in-Aid for JSPS Fellows (Grant No. 12J08652) from Japan Society for the Promotion of Science (JSPS), Japan. We are indebted to Yinwei Li for sharing the pseudopotentials and optimized structural parameters. We also thank Terumasa Tadano for fruitful discussions.

APPENDIX A: COMPUTATIONAL DETAIL

For the electronic and lattice-dynamical calculations, we used the pseudopotentials for S and H atoms implemented with the Troullier-Martin scheme [70], which are the same as those used in Ref. [34]. The plane-wave energy cutoff was set to 80 Ry, whereas the auxiliary cutoff for the dielectric function was 12.8 Ry. Conditions for the calculations of the charge density, dynamical matrix, electron-phonon coupling, dielectric function, and gap function are detailed in Table II.

APPENDIX B: NUMERICAL DATA OF THE CALCULATED VALUES OF T_c, λ, ω_{ln}, μ^*, AND α

Tables III–VII list the calculated values for T_c, λ, ω_{ln}, μ, and α.

TABLE II. Detailed settings for the calculations. The subscript "1" for **q** points denotes the mesh with displacement by half a grid step.

		$P1$ H_2S	$Cmca$ H_2S	$R3m$ H_3S	$Im\bar{3}m$ H_3S
Charge density	**k**	(12 12 8)	(12 12 4)	(16 16 16)	(16 16 16)
	Interpol.	First-order Hermine Gaussian [60] with width = 0.030 Ry			
Dynamical matrix	**k**	(12 12 8)	(12 12 4)	(16 16 16)	(16 16 16)
	q	$(6\,6\,4)_1$	$(6\,6\,2)_1$	$(8\,8\,8)_1$	$(8\,8\,8)_1$
	Interpol.	Optimized tetrahedron [58]			
Electron-phonon	**k**[a]	(12 12 8)	(24 24 8)	(32 32 32)	(32 32 32)
	Interpol.	Optimized tetrahedron [58]			
Dielectric function	**k** for bands crossing E_F[b]	(18 18 12)	(18 18 6)	(18 18 18)	(18 18 18)
	k for other bands	(6 6 4)	(6 6 2)	(6 6 6)	(6 6 6)
	q	(6 6 4)	(6 6 2)	(6 6 6)	(6 6 6)
	Unoccupied band num.	∼60	∼100	∼30	∼30
	Interpol.	Tetrahedron with the Rath-Freeman treatment [71]			
SCDFT gap function	Unoccupied band num.	25	45	19	19
	k for $\mathcal{K}^{el}$	(6 6 4)	(6 6 2)	(6 6 6)	(6 6 6)
	N_s for bands crossing E_F	4500	3000	6000	6000
	N_s for other bands	150	100	200	200
	Sampling error in T_c	∼9%	∼6%	∼5%	∼5%

[a]Electron energy eigenvalues and eigenfunctions were calculated on these auxiliary grid points.
[b]Electron energy eigenvalues were calculated on these auxiliary grid points.

TABLE III. Superconducting transition temperature T_c (K).

P (GPa)	130	150	170	190	210	230	250
H_2S	29.4	47.1	66.9	56.3	55.4	45.4	41.8
D_2S	25.0	38.2	55.7	46.7	45.0	37.9	35.7
H_3S	134	155	214		267	236	211
D_3S	103	119	163		206	180	164

TABLE IV. Electron-phonon coupling coefficient λ.

P (GPa)	130	150	170	190	210	230	250
H_2S	0.801	1.001	1.196	1.026	0.945	0.882	0.855
H_3S	1.843	2.067	2.599		2.582	2.263	1.970

TABLE V. Logarithmic moment of the Eliashberg function ω_{ln} (K).

P (GPa)	130	150	170	190	210	230	250
H_2S	913	914	968	1044	1097	1121	1124
H_3S	1037	1056	1058		1336	1447	1521

TABLE VI. Renormalized electron-electron Coulomb parameter μ^* estimated from the T_c calculated with the SCDFT gap equation.

P (GPa)	130	150	170	190	210	230	250
H_2S	0.155	0.165	0.174	0.166	0.152	0.158	0.159
H_3S	0.168	0.165	0.125		0.118	0.153	0.164

TABLE VII. Isotope effect coefficient α.

P (GPa)	130	150	170	190	210	230	250
H_2S	0.24	0.31	0.27	0.27	0.30	0.26	0.23
H_3S	0.38	0.39	0.40		0.38	0.40	0.37

[1] J. Bardeen, L. N. Cooper, and J. R. Schrieffer, Phys. Rev. **108**, 1175 (1957).

[2] A. F. Hebard, M. J. Rosseinsky, R. C. Haddon, D. W. Murphy, S. H. Glarum, T. T. M. Palstra, A. P. Ramirez, and A. R. Kortan, Nature (London) **350**, 600 (1991).

[3] J. Nagamatsu, N. Nakagawa, T. Muranaka, Y. Zenitani, and J. Akimitsu, Nature (London) **410**, 63 (2001).

[4] K. Shimizu, H. Ishikawa, D. Takao, T. Yagi, and K. Amaya, Nature (London) **419**, 597 (2002).

[5] V. V. Struzhkin, M. I. Eremets, W. Gan, H. K. Mao, and R. J. Hemley, Science **298**, 1213 (2002).

[6] E. A. Ekimov, V. A. Sidorov, E. D. Bauer, N. N. Mel'nik, N. J. Curro, J. D. Thompson, and S. M. Stishov, Nature (London) **428**, 542 (2004).

[7] H. Okazaki, T. Wakita, T. Muro, T. Nakamura, Y. Muraoka, T. Yokoya, S. Kurihara, H. Kawarada, T. Oguchi, and Y. Takano, Appl. Phys. Lett. **106**, 052601 (2015).

[8] N. W. Ashcroft, Phys. Rev. Lett. **21**, 1748 (1968).

[9] P. Cudazzo, G. Profeta, A. Sanna, A. Floris, A. Continenza, S. Massidda, and E. K. U. Gross, Phys. Rev. Lett. **100**, 257001 (2008).

[10] N. W. Ashcroft, Phys. Rev. Lett. **92**, 187002 (2004).

[11] J. Feng, W. Grochala, T. Jaroń, R. Hoffmann, A. Bergara, and N. W. Ashcroft, Phys. Rev. Lett. **96**, 017006 (2006).

[12] Y. Yao, J. S. Tse, Y. Ma, and K. Tanaka, Europhys. Lett. **78**, 37003 (2007).

[13] M. I. Eremets, I. A. Trojan, S. A. Medvedev, J. S. Tse, and Y. Yao, Science **319**, 1506 (2008).

[14] O. Degtyareva, J. E. Proctor, C. L. Guillaume, E. Gregoryanz, and M. Hanfland, Solid State Commun. **149**, 1583 (2009).

[15] X. Jin, X. Meng, Z. He, Y. Ma, B. Liu, T. Cui, G. Zou, and H. Mao, Proc. Natl. Acad. Sci. USA **107**, 9969 (2010).

[16] Y. Li, G. Gao, Y. Xie, Y. Ma, T. Cui, and G. Zou, Proc. Natl. Acad. Sci. USA **107**, 15708 (2010).

[17] J. A. Flores-Livas, M. Amsler, T. J. Lenosky, L. Lehtovaara, S. Botti, M. A. L. Marques, and S. Goedecker, Phys. Rev. Lett. **108**, 117004 (2012).

[18] T. Scheler, O. Degtyareva, M. Marqués, C. L. Guillaume, J. E. Proctor, S. Evans, and E. Gregoryanz, Phys. Rev. B **83**, 214106 (2011).

[19] X. F. Zhou, A. R. Oganov, X. Dong, L. Zhang, Y. Tian, and H. T. Wang, Phys. Rev. B **84**, 054543 (2011).

[20] D. Y. Kim, R. H. Scheicher, C. J. Pickard, R. J. Needs, and R. Ahuja, Phys. Rev. Lett. **107**, 117002 (2011).

[21] J. S. Tse, Y. Yao, and K. Tanaka, Phys. Rev. Lett. **98**, 117004 (2007).

[22] G. Gao, A. R. Oganov, P. Li, Z. Li, H. Wang, T. Cui, Y. Ma, A. Bergara, A. O. Lyakhov, T. Iitaka, and G. Zou, Proc. Natl. Acad. Sci. USA **107**, 1317 (2010).

[23] I. Goncharenko, M. I. Eremets, M. Hanfland, J. S. Tse, M. Amboage, Y. Yao, and I. A. Trojan, Phys. Rev. Lett. **100**, 045504 (2008).

[24] G. Gao, A. R. Oganov, A. Bergara, M. Martinez-Canales, T. Cui, T. Iitaka, Y. Ma, and G. Zou, Phys. Rev. Lett. **101**, 107002 (2008).

[25] R. Szczęśniak, A. P. Durajski, and D. Szczęśniak, Solid State Commun. **165**, 39 (2013).

[26] G. Gao, H. Wang, A. Bergara, Y. Li, G. Liu, and Y. Ma, Phys. Rev. B **84**, 064118 (2011).

[27] R. Szczęśniak and A. P. Durajski, Supercond. Sci. Technol. **27**, 015003 (2014).

[28] H. Wang, J. S. Tse, K. Tanaka, T. Iitaka, and Y. Ma, Proc. Natl. Acad. Sci. USA **109**, 6463 (2012).

[29] D. C. Lonie, J. Hooper, B. Altintas, and E. Zurek, Phys. Rev. B **87**, 054107 (2013).

[30] Z. Wang, Y. Yao, L. Zhu, H. Liu, T. Iitaka, H. Wang, and Y. Ma, J. Chem. Phys. **140**, 124707 (2014).

[31] D. Zhou, X. Jin, X. Meng, G. Bao, Y. Ma, B. Liu, and T. Cui, Phys. Rev. B **86**, 014118 (2012).

[32] D. Y. Kim, R. H. Scheicher, H. Mao, T. W. Kang, and R. Ahuja, Proc. Natl. Acad. Sci. USA **107**, 2793 (2010).

[33] G. Gao, R. Hoffmann, N. W. Ashcroft, H. Liu, A. Bergara, and Y. Ma, Phys. Rev. B **88**, 184104 (2013).

[34] Y. Li, J. Hao, H. Liu, Y. Li, and Y. Ma, J. Chem. Phys. **140**, 174712 (2014).

[35] D. Duan, Y. Liu, F. Tian, D. Li, X. Huang, Z. Zhao, H. Yu, B. Liu, W. Tian, and T. Cui, Sci. Rep. **4**, 6968 (2014).

[36] A. P. Drozdov, M. I. Eremets, and I. A. Troyan, arXiv:1412.0460.

[37] J. E. Hirsch and F. Marsiglio, Physica C **511**, 45 (2015).

[38] A. P. Durajski, R. Szczęśniak, and Y. Li, Physica C **515**, 1 (2015).

[39] N. Bernstein, C. S. Hellberg, M. D. Johannes, I. I. Mazin, and M. J. Mehl, Phys. Rev. B **91**, 060511(R) (2015).

[40] D. Duan, X. Huang, F. Tian, D. Li, H. Yu, Y. Liu, Y. Ma, B. Liu, and T. Cui, Phys. Rev. B **91**, 180502(R) (2015).

[41] D. A. Papaconstantopoulos, B. M. Klein, M. J. Mehl, and W. E. Pickett, Phys. Rev. B **91**, 184511 (2015).

[42] A. B. Migdal, Zh. Eksp. Teor. Fiz. **34**, 1438 (1958) [Sov. Phys. JETP **7**, 996 (1958)].

[43] P. B. Allen and R. C. Dynes, Phys. Rev. B **12**, 905 (1975).

[44] P. Morel and P. W. Anderson, Phys. Rev. **125**, 1263 (1962).

[45] J. W. Garland, Phys. Rev. Lett. **11**, 114 (1963).

[46] J. P. Carbotte, Rev. Mod. Phys. **62**, 1027 (1990).

[47] G. M. Eliashberg, Zh. Eksp. Teor. Fiz. **38**, 966 (1960) [Sov. Phys. JETP **11**, 696 (1960)]; D. J. Scalapino, in *Superconductivity*, edited by R. D. Parks (Dekker, New York, 1969), Vol. 1; J. R. Schrieffer, *Theory of Superconductivity* (Westview Press, Boulder, CO, 1971).

[48] M. Lüders, M. A. L. Marques, N. N. Lathiotakis, A. Floris, G. Profeta, L. Fast, A. Continenza, S. Massidda, and E. K. U. Gross, Phys. Rev. B **72**, 024545 (2005).

[49] M. A. L. Marques, M. Lüders, N. N. Lathiotakis, G. Profeta, A. Floris, L. Fast, A. Continenza, E. K. U. Gross, and S. Massidda, Phys. Rev. B **72**, 024546 (2005).

[50] R. Akashi and R. Arita, Phys. Rev. Lett. **111**, 057006 (2013).

[51] R. Akashi and R. Arita, J. Phys. Soc. Jpn. **83**, 061016 (2014).

[52] Y. Takada, J. Phys. Soc. Jpn. **45**, 786 (1978).

[53] J. P. Perdew, K. Burke, and M. Ernzerhof, Phys. Rev. Lett. **77**, 3865 (1996).

[54] P. Giannozzi, S. Baroni, N. Bonini, M. Calandra, R. Car, C. Cavazzoni, D. Ceresoli, G. L. Chiarotti, M. Cococcioni, I. Dabo, A. Dal Corso, S. Fabris, G. Fratesi, S. de Gironcoli, R. Gebauer, U. Gerstmann, C. Gougoussis, A. Kokalj, M. Lazzeri, L. Martin-Samos, N. Marzari, F. Mauri, R. Mazzarello, S. Paolini, A. Pasquarello, L. Paulatto, C. Sbraccia, S. Scandolo, G. Sclauzero, A. P. Seitsonen, A. Smogunov, P. Umari, and R. M. Wentzcovitch, J. Phys.: Condens. Matter **21**, 395502 (2009); http://www.quantum-espresso.org/

[55] S. Baroni, S. de Gironcoli, A. Dal Corso, and P. Giannozzi, Rev. Mod. Phys. **73**, 515 (2001).

[56] R. Akashi and R. Arita, Phys. Rev. B **88**, 014514 (2013).
[57] R. Akashi, K. Nakamura, R. Arita, and M. Imada, Phys. Rev. B **86**, 054513 (2012).
[58] M. Kawamura, Y. Gohda, and S. Tsuneyuki, Phys. Rev. B **89**, 094515 (2014).
[59] We employed the approximation $\int d\nu \simeq 2\int_0^{\nu_{\max}} d\nu$ for the numerical ν-integral with $\nu_{\max} = 70$ eV. The high-frequency contribution $\int_{\nu_{\max}}^{\infty} d\nu$ was estimated analytically with the approximation $W_{n\mathbf{k}n'\mathbf{k}'}(i\nu) \simeq W_{n\mathbf{k}n'\mathbf{k}'}(i\nu_{\max})$.
[60] M. Methfessel and A. T. Paxton, Phys. Rev. B **40**, 3616 (1989).
[61] A. Floris, A. Sanna, S. Massidda, and E. K. U. Gross, Phys. Rev. B **75**, 054508 (2007).
[62] A. Floris, G. Profeta, N. N. Lathiotakis, M. Lüders, M. A. L. Marques, C. Franchini, E. K. U. Gross, A. Continenza, and S. Massidda, Phys. Rev. Lett. **94**, 037004 (2005); A. Floris, A. Sanna, M. Lüders, G. Profeta, N. N. Lathiotakis, M. A. L. Marques, C. Franchini, E. K. U. Gross, A. Continenza, and S. Massidda, Physica C **456**, 45 (2007).
[63] A. Sanna, G. Profeta, A. Floris, A. Marini, E. K. U. Gross, and S. Massidda, Phys. Rev. B **75**, 020511(R) (2007).
[64] G. Profeta, C. Franchini, N. N. Lathiotakis, A. Floris, A. Sanna, M. A. L. Marques, M. Lüders, S. Massidda, E. K. U. Gross, and A. Continenza, Phys. Rev. Lett. **96**, 047003 (2006).
[65] J. A. Flores-Livas, A. Sanna, and E. K. U. Gross, arXiv:1501.06336.
[66] In Ref. [65] (i) they used modified forms for the phonon part of the SCDFT kernels, though the details of the modification have not yet been published (see Ref. [56] in Ref. [65]), (ii) they did not include the plasmon-induced dynamical effect, and (iii) their calculation was based on the local-density approximation, [67,68] which yielded a $R3m$-$Im\bar{3}m$ structural transition point that is slightly different from that with the generalized-gradient approximation [35].
[67] D. M. Ceperley and B. J. Alder, Phys. Rev. Lett. **45**, 566 (1980).
[68] J. P. Perdew and A. Zunger, Phys. Rev. B **23**, 5048 (1981).
[69] I. Errea, M. Calandra, C. J. Pickard, J. Nelson, R. J. Needs, Y. Li, H. Liu, Y. Zhang, Y. Ma, and F. Mauri, Phys. Rev. Lett. **114**, 157004 (2015).
[70] N. Troullier and J. L. Martins, Phys. Rev. B **43**, 1993 (1991); http://www.abinit.org/downloads/psp-links/psp-links/gga_fhi
[71] J. Rath and A. J. Freeman, Phys. Rev. B **11**, 2109 (1975).